

Identification of aerosols by their backscattered Mueller images

Changhui Li and George W. Kattawar

*Department of Physics, Texas A&M University,
College Station, TX, 77843
kattawar@tamu.edu*

Ping Yang

*Department of Atmospheric Sciences, Texas A&M University,
College Station, TX, 77843*

Abstract: We have simulated the elastic light scattering by small dielectric particles with different shapes as well as different compositions. Backscattered angularly resolved Mueller images are obtained from the simulation. Our results show that the images are not only sensitive to the shape, size and orientation of the particle, but also sensitive to the composition. Thus the Mueller images act in reality like a Mueller-microscope, and can thus lead to the detection and classification of aerosols.

©2006 Optical Society of America

OCIS codes: (290.650) Backscattering; (170.0170) Medical optics and biotechnology; (290.5850) Scattering, particles; (100.5010) Pattern recognition and feature extraction; (110.180) Microscopy; (260.5430) Physical optics: Polarization.

References

1. D. A. Henderson, "The looming threat of bioterrorism," *Science* **283**, 1279-1282 (1999).
2. M. O. Scully, G. W. Kattawar, R. P. Lucht, T. Opatrny, H. Pilloff, A. Rebane, A. V. Sokolov, and M. S. Zubairy, "FAST CARS: Engineering a laser spectroscopic technique for rapid identification of bacterial spores," *Proc. Natl. Acad. Sci. USA* **99**, 10994-11001 (2002).
3. R. G. Pinnick, S. C. Hill, P. Nachman, J. D. Pendleton, G. L. Fernandez, M. W. Mayo, and J. G. Bruno, "Fluorescence particle counter for detecting airborne bacteria and other biological particles," *Aerosol. Sci. Technol.* **23**, 653-664 (1995).
4. B. D. Cameron, M. J. Rakovic, M. Mehrbeoglu, G. W. Kattawar, S. Rastegar, L. V. Wang, and G. L. Cot, "Measurement and calculation of the two-dimensional backscattering Mueller matrix of a turbid medium," *Opt. Lett.* **23**, 485-487 (1998).
5. A. A. Nezhuvungal, Y. Li, H. Anumula, B. D. Cameron, "Mueller matrix optical imaging with application to tissue diagnostics," *Proc. SPIE* **4961**, 67-146 (2003).
6. Y. L. Pan, K. B. Aptowicz, R. K. Chang, M. Hart, and J. D. Eversole, "Characterizing and monitoring respiratory aerosols by light scattering," *Opt. Lett.* **28**, 589 (2003).
7. K. S. Yee, "Numerical solution of initial boundary problems involving Maxwell's equations in isotropic media," *IEEE Trans. Antennas Propag.* **AP-14**, 302-307 (1966).
8. Yang, P., K. N. Liou, M. I. Mishchenko, and B.-C. Gao, "An efficient finite-difference time domain scheme for light scattering by dielectric particles: application to aerosols," *Appl. Opt.* **39**, 3727-3737 (2000).
9. A. Taflove and S. Hagness, *Computational Electrodynamics: the Finite-Difference Time-Domain Method* (Artech, Boston, MA, 2000).
10. Philip J. Wyatt, "Differential Light Scattering: a Physical Method for Identifying Living Bacterial Cells," *Appl. Opt.* **7**, 1879 (1968).

1. Introduction

Bioaerosols such as spores, pollens, some viruses and cells have dimensions of the order of micrometers. There are large variations in both the morphology and composition of these

particles. In recent years the detection and classification of bioaerosols, such as anthrax, has gained the attention of many research groups because of bioterrorism threats [1]. Of all the detection methods proposed thus far, DNA analysis is perhaps the most accurate. However DNA analysis not only requires complex equipment, it also takes a long time to complete. In reality, hazardous bioaerosols may be mixed with similar but benign particles, it then takes even longer in detection time for DNA analysis to separate the benign from the hazardous ones. Many methods have been applied and are under further research to speed up the analysis procedure, such as FASTCARs [2], fluorescence [3], etc.

Images based on the Mueller matrix have previously been explored in studying optical properties of turbid media [4, 5], such as tissues. In this paper, we study light scattered from isolated single particles. With recent developments in detection schemes, complete backscattered light can be detected [6]. We have computed the backscattered Mueller matrix, and from it constructed angularly resolved Mueller images. There are three models used in this paper; namely, a homogenous ellipsoid, an ellipsoid with core, and homogenous cylinders. Since the sizes of these particles are comparable with the incident wavelength, geometric optics is not an option. We therefore used the finite-difference time-domain (FDTD) [7-9] technique to perform the numerical simulation involved in this study.

2. Models and image construction

In our simulation, the models are constructed as shown in Fig. 1. They are: one homogenous ellipsoid (Fig. 1(a)), one spore (Fig. 1(b)) (same shape as the Fig. 1(a) but with inhomogeneous compositions) and homogenous cylinders with different heights (Fig. 1(c)). The refractive indexes for the homogenous ellipsoid and cylinder are $m=1.34$. In case of the spore model, the refractive index is chosen according to Fig. 1(d) based on the relative radial distance from the boundary. As described in [10], the spore model used in this paper represents a spore with a core in the center and a single layer coat. In our simulation, the scatterers are placed in the air, which has refractive index $m=1.0$.

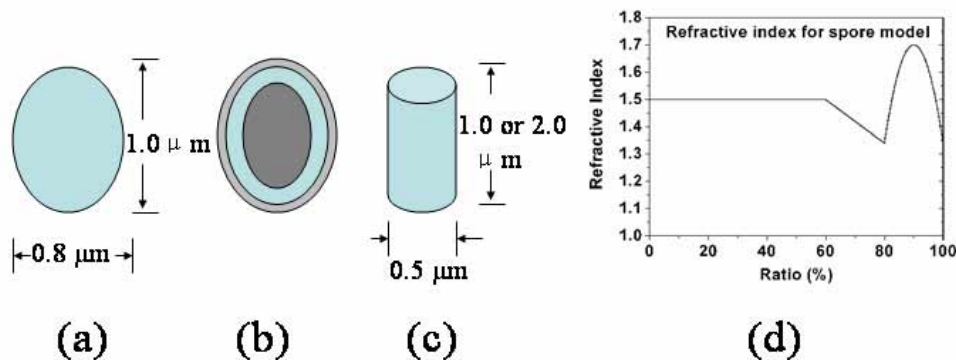


Fig. 1. Particle geometries used in this study: (a) a homogenous ellipsoid with a major axis of $1.0 \mu\text{m}$ and a minor axis of $0.8 \mu\text{m}$; (b) the same ellipsoid with a centered core and one layer coat; (c) homogenous cylinders with heights $1.0 \mu\text{m}$ or $2.0 \mu\text{m}$, and width $0.5 \mu\text{m}$; (d) the refractive index for (b).

The backscattered region (polar angle from 90 to 180 degree) is the one we chose in this paper. An actual experimental setup has been done in [6] as shown in Fig. 2(a), in which almost all the backscattered light can be detected.

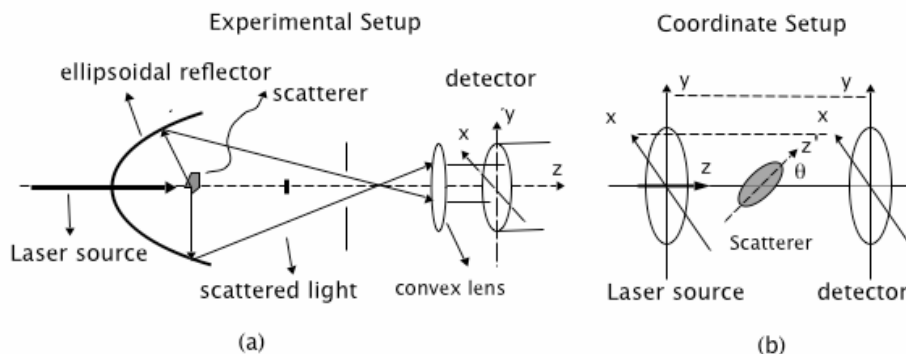


Fig. 2. (a) An experimental setup to measure the backscattered light in [6]. This experimental setup collects most of the backscattered light and projects it to the detector. (b) Coordinates used in this paper. The scatterer is fixed in the yz-plane, θ is the angle between the symmetry axis of the scatterer and z axis.

The Mueller matrix is the transformation matrix between the incident Stokes vector and the outgoing Stokes vector. Since the Stokes vector is only meaningful when defined with respect to a coordinate system, Mueller matrix elements also depend on the coordinate system. Fig. 2(b) shows the coordinate system used in this paper, the x, y, and z axes form a right-handed Cartesian coordinate system, where z is the direction of the incident illumination beam. To simplify the simulation process, the particle's symmetry axis is fixed in the yz plane. Mueller matrix elements are dependent on particle orientation (denoted by θ) and the scattering angle in the coordinate system defined here. For any given θ , the constructed images are angularly resolved images. The image has a disk shape with 180-degree polar angle at the center of total backscattering and the 90-degree polar angle at the boundary. The polar angle is uniformly divided along the radius in the image. The uniform division of the polar angle may not be satisfied in the experimental setup as shown in the Fig. 2(a).

3. Results of simulation

The Mueller matrix ($M=\{m_{ij}(\theta,\phi), i,j=1,2,3,4\}$) is a 4x4 matrix and therefore the corresponding complete Mueller images contain 16 sub-images. In this paper, the reduced Mueller matrix is used, which means all values except m_{11} are normalized by m_{11} . Thus all matrix elements except m_{11} are in the region (-1,1). In Fig. 3, an example of the complete Mueller images is shown. These images show the simulation results of the homogenous ellipsoid as in Fig. 1(a) with an orientation angle of 90° (broadside illumination). The first image element m_{11} represents the angular distribution of scattered light intensity with an unpolarized illuminating beam. The color bar of m_{11} represents the values in the sense of the following equation:

$$\sigma = \frac{1}{k^2} \int m_{11}(\theta, \phi) d\Omega,$$

where the integral is over the whole 4π steradian solid angle; σ is the scattering cross section, which equals to $2.23 \mu\text{m}^2$ in this case for unpolarized incident light; k is the wave vector defined as $k=2\pi/\lambda$ and λ is the wavelength. Since we are interested in the pattern character, values for m_{11} in the following figures are not specified although the color scale in the image is from blue to red corresponding to the minimum and maximum values of m_{11} in backscattered region. The color used in all the other element images except m_{11} scales from -1 to 1. It is worthy to note that values are zero along x and y-axis for elements (m_{13} , m_{14} , m_{23} , m_{24} , m_{31} , m_{32} , m_{41} , and m_{42}), which is because the particle simulated has mirror symmetry with respect to xz and yz-plane.

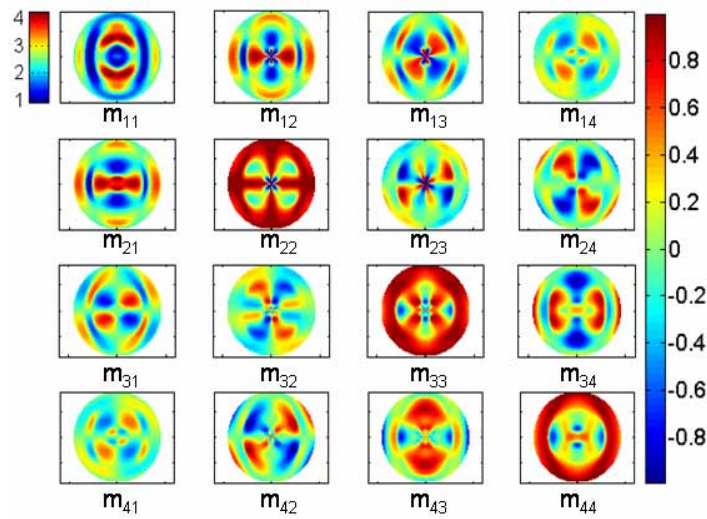


Fig. 3. A complete set of Mueller images for broadside illumination of the homogenous ellipsoid with a major axis of $1.0 \mu\text{m}$ and a minor axis of $0.8 \mu\text{m}$, the refractive index is 1.34 and the illuminating wavelength is $0.5 \mu\text{m}$.

As mentioned earlier, Mueller images depend on the orientation of the scatterer, each orientation has a unique 4×4 Mueller image. In the following, three orientations with polar angle $\theta=0^\circ$, 30° and 90° are simulated. To compare the differences in Mueller images of different shapes and compositions, m_{11} and m_{44} are used as representatives for Mueller images.

Figure 4 shows the comparison between the homogenous ellipsoid and the spore model. For Mueller images of m_{11} and m_{44} there are significant differences. The presence of the core and the coat greatly change the backscattered image pattern. The spore gives more fine structure in the m_{44} images. One can also see the scattering patterns change with the orientation angle. From these patterns, it should be possible to retrieve the composition and orientation information.

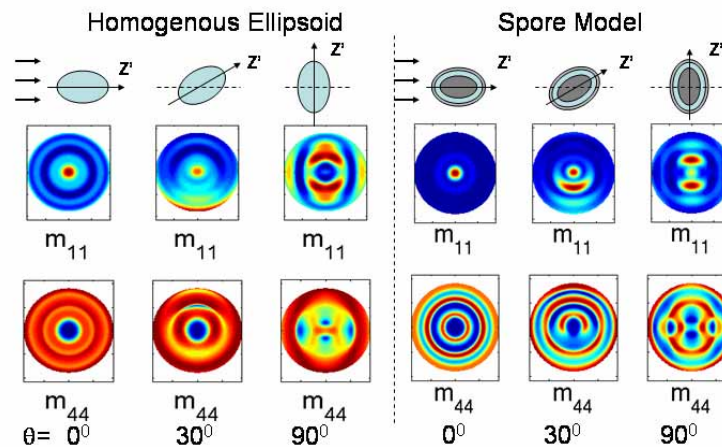


Fig. 4. Comparison for Mueller elements m_{11} and m_{44} between homogenous ellipsoid and spore at different orientations. Both spores have a major axis of $1.0 \mu\text{m}$ and a minor axis of $0.8 \mu\text{m}$, the illuminating wavelength is $0.5 \mu\text{m}$.

Figure 5 compares the scattering image patterns for the homogenous ellipsoid, the spore with core and coat and a homogenous cylinder with height 1.0 micrometer. They are all broadside illuminated, i.e., $\theta=90^\circ$. Although the three small particles are similar in size scale compared with the wavelength of the illuminating beam, there are distinct differences in the patterns between the cylinder's images and the ellipsoid's. One can easily distinguish the cylinder shape from the ellipsoid shape.

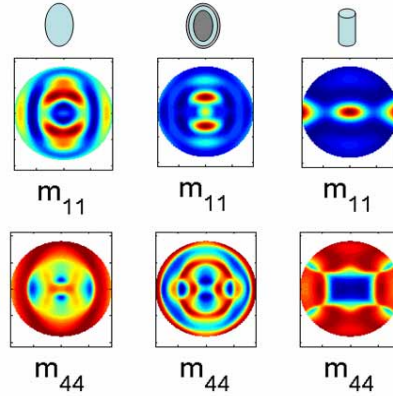


Fig. 5. Comparison for Mueller element m_{11} and m_{44} between the homogenous ellipsoid, the spore and the homogenous cylinder for broadside illumination.

To study how the size affects the scattering patterns, we doubled the height of the cylinder while keeping the radius unchanged. The results are shown in Fig. 6. Overall the patterns for these two cylinders are similar. The increase in the height brings more fine structure. Size information could possibly be derived from this fine structure.

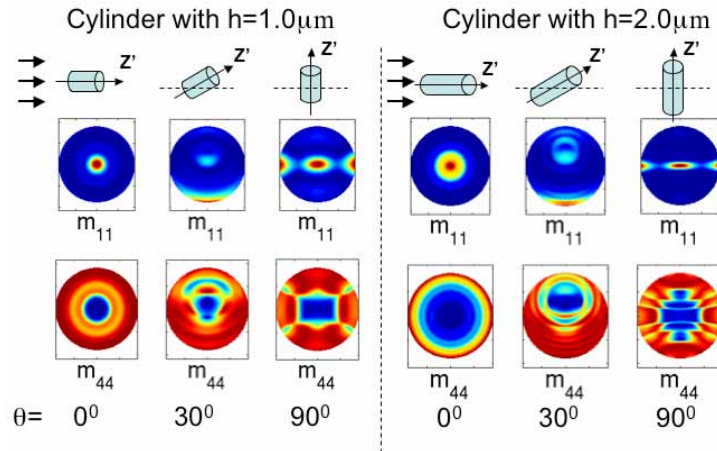


Fig. 6. Comparison for Mueller element m_{11} and m_{44} between homogenous cylinders with different heights of 1.0 μm and 2.0 μm , and the same diameter of 0.5 μm , refractive index is 1.34 and illuminating wavelength is 0.5 μm .

To compare with forward scattering results, in Fig. 7 we calculated forward scattered Mueller images for the same case as used in Fig. 5. There is less information contained in the forward scattering pattern compared with results in Fig. 5. For three m_{11} images, their patterns look similar, which means that forward scattering m_{11} is not as sensitive to the shape and internal structures as for the m_{44} images. Although there are some differences in regions away

from the center for m_{44} , the differences are not as distinct as backscattered images. This is the reason we feel backscattering is more important in classifying aerosols.

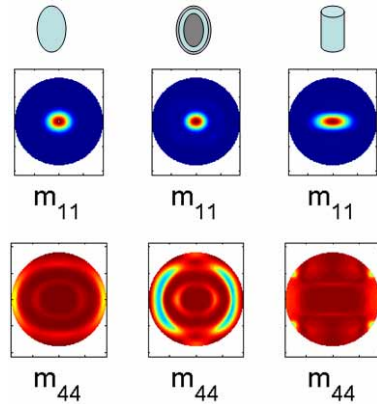


Fig. 7. Same as Fig. 5 except for the Mueller images for forward scattering.

4. Discussions and conclusions

In this paper, backscattered Mueller images are simulated for several small dielectric particles whose sizes are comparable to the wavelength of the illuminating light. Compared with forward scattering results as shown in Fig. 7, backscattered Mueller images are much more sensitive to the shape, size and composition of the particle. Even in the simplest case where only the scattered intensity is detected with an unpolarized illuminating source, backscattered intensity image (m_{11}) still shows more variation between different cases. However, when the polarization is taken into account, the other Mueller images contain more pattern variations.

To obtain complete identification would require solving the inverse problem, which will be quite difficult to do. However even without inverse methods, one can setup databases for known particles and do pattern recognition to distinguish different kinds of particles.

In addition to the classification of particles, the results shown in this paper can be applied to rapid detection of hazardous biological agents. Together with proper experimental setup (such as the one shown in [6]), pattern recognition can be used to identify particles having similar Mueller images as the hazardous biological agents stored in the database. The selected particles can then undergo further analysis by other methods, such as DNA analysis. The sample number is greatly minimized as well as the total detection time. Since this method uses the strong elastic scattered signals, it does not require sophisticated equipment for signal amplification.

The simulations in this paper are only for a single particle. It is straightforward to apply this simulation to clusters. We also want to explore the possibility of using two wavelengths and looking at differences in the Mueller images.

Acknowledgments

This research was partially supported by the Office of Naval Research under contracts N00014-02-1-0478, the Defense Advanced Research Projects Agency, and the Robert A. Welch Foundation Grant No. A1261. Ping Yang's effort is supported by the National Science Foundation (ATM-0239605) and a research grant (NNG04GL24G) from NASA Radiation Sciences Program managed by Dr. Hal Maring (previously by Dr. Donald Anderson).